

Noise Measurements in Supersonic Jets Treated with the Mach Wave Elimination Method

Dimitri Papamoschou* and Marco Debiasi†
University of California, Irvine, Irvine, California 92717-3975

We report noise measurements for perfectly expanded coaxial jets composed of a supersonic primary stream at velocity of 920 m/s and a coflow stream at conditions designed to prevent formation of Mach waves. Both the primary and secondary streams consisted of helium-air mixtures to simulate approximately the conditions of hot flows. The resulting sound field was compared to that emitted by a single jet at the conditions of the primary stream. Overall sound pressure levels (OASPL) and noise spectra were obtained at many radial and azimuthal positions around the jet exit. Equal-thrust comparisons were made by using geometric scaling. At equal thrust, Mach wave elimination reduced the near-field OASPL by 11 dB and the far-field OASPL by 5 dB. The mid-to-high-frequency region of the spectrum, which is most pertinent to aircraft noise, was reduced by 20 dB in the near field and by 9 dB in the far field. It is shown that Mach waves account for at least 85% of the sound field most relevant to aircraft noise.

I. Introduction

MACH wave radiation is an integral feature of jets with velocity in excess of about 450 m/s. It is caused by the supersonic convection of turbulent eddies in the proximity of the jet exit. Because of its relevance to the takeoff noise of supersonic aircraft, it has been the subject of numerous experimental^{1,2} and theoretical³⁻⁵ works. Photographic evidence, directivity of the measured sound, and computational results indicate that Mach waves constitute an important source of noise in supersonic jets.

However, there have been few attempts to distinguish Mach wave emission from other sources of noise, namely, conventional quadrupole noise and shock-induced noise (screech and broadband) in imperfectly expanded jets. Although shock noise can be eliminated by perfect expansion of the jet, separating Mach wave emission from quadrupole noise is very difficult. The same feature responsible for Mach wave emission, high velocity, also produces strong quadrupole sources, particularly in the region downstream of the potential core where large eddies dominate. One notable work that attempted to differentiate between these two sources of sound is by Bishop et al.,⁶ where a sound absorbing screen with a hole was used to separate sources of sound upstream and downstream of the end of the potential core. The authors concluded that Mach waves account for as much as 20 dB of the total noise field. We must note, however, that the Ref. 6 jet was highly underexpanded, hence emitting strong screech noise that the screen undoubtedly suppressed by impeding the feedback loop essential to screech generation.⁷ This casts doubt on their assessment of the Mach wave content of noise and illustrates the difficulty of separating sources of sound in an experiment. At this stage of our understanding of jet noise, the fraction of noise attributable to Mach waves, especially in the far field, is not known. Moreover, it has been suggested that the frequency of Mach waves may be too high to contribute significantly to the engine noise perceived by humans.⁸

Recently, it was demonstrated that Mach waves can be eliminated by addition of a layer of coflow around the primary jet such that the primary eddies become subsonic with respect to the coflow and the coflow eddies are subsonic with respect to the ambient.⁹ An empirical model for the eddy convective velocity U_c , based on its direct

measurement in shear layers,¹⁰ led to the appropriate conditions of the coflow in terms of its temperature and Mach number (see Fig. 1). The model is complex, but a rough approximation would be that eddies of the inner shear layer propagate with 80% of the jet velocity and those of the outer shear layer with 60% of the coflow velocity. In an engine, the coflow could be supplied by the fan stream or by an ejector.

Fundamental studies of the noise characteristics of pressure-matched coaxial supersonic jets, such as those investigated here, have been scarce. Experiments on the noise of coaxial jets, published in the archival literature, have been confined to either subsonic speeds or to supersonic underexpanded conditions. An overview of subsonic experiments is given by Tanna,¹¹ who compared coaxial jets with normal velocity profile to those with inverted velocity profile (IVP) and concluded that IVP jets are quieter in terms of overall sound pressure level but noisier in terms of perceived noise level. Dosanjh et al.¹² investigated coannular supersonic jets with IVP and observed significant noise reduction at certain combinations of pressure ratios for the inner and outer streams at which the internal shock structure of the jet was significantly weakened. A recent theoretical study of coaxial jets by Dahl and Morris¹³ shows that instability waves with supersonic phase speeds constitute the dominant source of mixing noise radiated into the downstream arc of the jet. Depending on the velocity ratio, the dominant instability develops in the inner shear layer or in the outer shear layer. Dahl and Morris' work did not encompass conditions under which both inner- and outer-layer instabilities are intrinsically subsonic, leading to Mach wave elimination.

Experimental evidence of Mach wave elimination has so far been based on schlieren photography.⁹ The present study uses sound measurements to evaluate application of the Mach wave elimination method on a small-scale, perfectly expanded jet at exit conditions that match the Mach number, density, and velocity of a typical supersonic engine. The experiments also shed some light on the questions raised earlier, i.e., what fraction of the emitted sound is due to Mach waves and which portion of the frequency spectrum do they influence?

II. Flow Apparatus

Experiments were conducted in a coaxial jet facility, a detailed description of which can be found in Ref. 9. Mixtures of helium and air were supplied to a concentric nozzle arrangement shown in Fig. 2. The inner nozzle, of 12.7 mm exit diameter, was designed by the method of characteristics for exit Mach number $M_1 = 1.5$. The outer nozzle formed a smooth contraction terminating in an exit diameter of 25.4 mm. Precisely metered mixtures of helium and air were supplied to the nozzles, which exhausted into ambient,

Presented as Paper 98-0280 at the AIAA 36th Aerospace Sciences Meeting, Reno, NV, Jan. 12-15, 1998; received April 5, 1998; revision received Oct. 21, 1998; accepted for publication Oct. 26, 1998. Copyright © 1998 by Dimitri Papamoschou and Marco Debiasi. Published by the American Institute of Aeronautics and Astronautics, Inc., with permission.

*Professor, Department of Mechanical and Aerospace Engineering. E-mail: dpapamos@uci.edu. Member AIAA.

†Research Assistant, Department of Mechanical and Aerospace Engineering. Member AIAA.

Table 1 Flow conditions

Case	M_1	U_1 , m/s	T_1/T_∞^a	M_2	U_2 , m/s	T_2/T_∞^a	\dot{m}_2/\dot{m}_1	F_{1+2}/F_1
A	1.5	920	2.8	0.00	0	1.0	0	1.00
B	1.5	920	2.8	0.83	400	1.7	2.1	1.92
C	1.5	920	2.8	0.15	110	4.0	2.0	1.15
D	1.5	700	1.8	0.00	0	1.0	0	1.00

^a T , effective temperature.

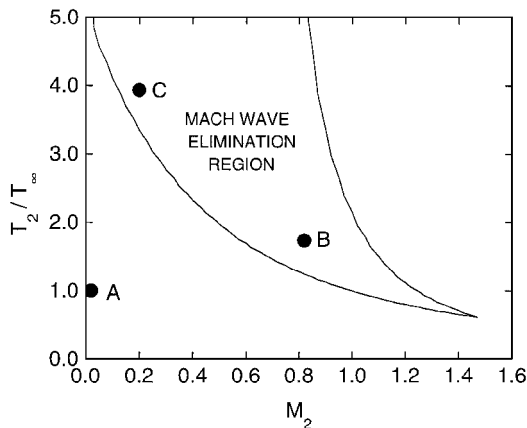


Fig. 1 Mach wave elimination region for a jet with $M_1 = 1.5$ and $T_1/T_\infty = 2.8$; location of cases A–C is indicated.

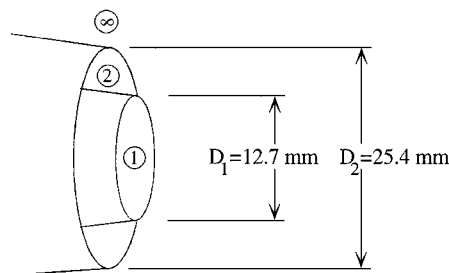


Fig. 2 Coaxial jet geometry.

still air. The total pressure of the inner (primary) flow was set at 375 kPa, resulting in a pressure-matched jet. Special care was taken to maintain the total pressure to within 1% of the pressure-matched value. For the majority of the experiments described here, the outer (coflow) stream was supplied at a total pressure of 160 kPa, resulting in an exit Mach number $M_2 = 0.83$. Helium–air mixtures allow variation of the gas constant R and, thus, of the velocity at fixed Mach number and fixed total temperature. A jet composed of helium–air mixture simulates reasonably accurately the speed of sound, velocity, and growth rate of a hot jet at the same density ratio.^{9,14} In this experiment, the mixtures were accurately metered so that the uncertainty in the gas constant was less than 5%. The total temperature of the gas mixture was around 300 K. The exit density can be translated to the temperature of the simulated hot jet via the relation $T/T_\infty = \rho_\infty/\rho$ (Ref. 9). Our baseline case has a jet velocity $U_1 = 920$ m/s, which is typical of supersonic engines. The automated facility was equipped with pressure transducers (Setra model 280), which recorded the total pressures in the primary and coflow streams, as well as the pressure from a pitot probe traversing along the jet centerline. A schlieren system, illuminated by a 20-ns spark gap (Xenon Nanolamp), enabled frozen visualization of the flow. Table 1 summarizes the flow conditions. The last column indicates the calculated ratio of the thrust of the combined flow over the thrust of the primary flow. The Reynolds number of the primary jet was 3.8×10^5 for cases A–C and 4.9×10^5 for case D. Cases A and B comprise the majority of the experiments, whereas cases C and D represent limited investigations to obtain important reference points. Figure 1 shows the location of cases A–C on the Mach wave elimination diagram.

III. Sound Measurement

Data Collection

The jet noise was recorded by a 1/8th-in. condenser microphone connected to a preamplifier and power supply (Brüel and Kjær Models 4138, 2670, and 5935L, respectively). The microphone has a frequency response of 150 kHz and was sampled at 400 kHz by a fast analog-to-digital board (National Instruments AT-MIO-16E1) installed in a Pentium Pro computer. Each recording consisted of 54,280 samples (135 ms), corresponding to passage of about 10,000 eddies the size of the inner-jet diameter. Occasionally, the sample size was increased to 131,072, but there was no significant difference seen in the results. The signal was high-pass filtered at 500 Hz by a Butterworth filter to remove spurious low-frequency noise. The power spectrum of each recording was computed using a 512-point fast Fourier transform with a full Hanning window. The microphone was calibrated daily before each series of recordings (Brüel and Kjær model 4231 calibrator).

Sound measurements were conducted inside an anechoic chamber, approximately 8 m³ in internal size, lined with acoustic wedges (Sonex) with an absorption coefficient higher than 0.99 for frequencies above 500 Hz. Figure 3 provides a cutaway of the chamber and shows the jet and microphone positions. The microphone was mounted on an arm that pivoted around an axis passing through the center of the jet exit. This arrangement enabled sound measurement at a variety of radial r and polar θ positions, r ranging from 0.038 to 1.52 m and θ ranging from 20 to 100 deg, measured counterclockwise from the jet axis. For very large radial distances, the range of polar angles was limited due to interference with the chamber's walls.

Data Processing

Signal processing yielded two important noise parameters, the sound pressure level (SPL) spectrum, which shows the distribution of noise vs frequency, and the overall sound pressure level (OASPL), which describes the contribution of all measured frequencies. The units for both quantities are decibels. The OASPL is defined as

$$\text{OASPL} = 20 \log_{10}(p'_{\text{rms}}/p_{\text{ref}}) \quad (1)$$

where p'_{rms} is the root mean square pressure fluctuation and $p_{\text{ref}} = 20 \mu\text{Pa}$ is the commonly used reference pressure. Alternatively, the OASPL can be computed in the frequency domain by

$$\text{OASPL} = 10 \log_{10} \int_0^\infty S(f) df \quad (2)$$

where $S(f)$ is the power spectrum of the pressure fluctuation, normalized such that

$$\int_0^\infty S(f) df = \frac{\langle p'^2 \rangle}{p_{\text{ref}}^2} = \frac{p_{\text{rms}}^2}{p_{\text{ref}}^2}$$

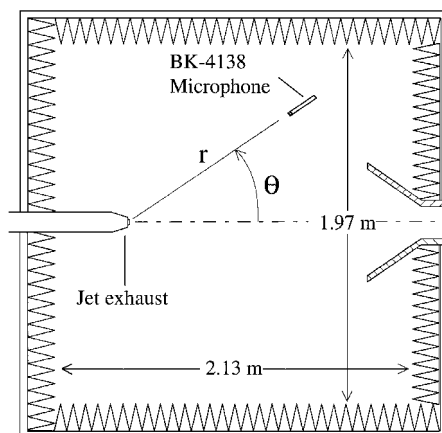


Fig. 3 Anechoic chamber and positioning of jet and microphone.

where $\langle \rangle$ denotes the time average. The corresponding SPL spectrum is given by

$$\text{SPL}(f) = 10 \log_{10} S(f) \quad (3)$$

Before calculating these quantities, the microphone signal must be corrected for the frequency response and the free-field response. Both corrections take place in the frequency domain according to data provided by the microphone manufacturer (Brüel and Kjær). Whereas the frequency-response correction is minor, the free-field correction can be significant for $f > 50$ kHz, where the sound wavelength becomes of the same order as the dimensions of the slots of the microphone protective grid and, as a result, the grid influences the measurement of sound. The free-field correction depends on the frequency f and the angle ϕ between the sound propagation vector and the microphone axis. Because it is an important correction, we independently verified the Brüel and Kjær correction curves for $\phi = 0$ and 90 deg by changing the microphone incidence angle in the far field, where the sound propagation vector is in the radial direction. For the near field ($r/D_1 < 12$), we assumed that sound propagates normal to the Mach waves, which we visualized, except for $\theta > 60$ deg, where Mach waves do not exist and where the wave fronts were assumed to be spherical.

Another complication of working at very high frequencies is atmospheric absorption of sound. For given temperature, pressure, and humidity, absorption increases with f^2 , and so it has a much larger impact on subscale tests than on full-size tests. In our experiments, absorption of the 100-kHz component of noise ranged from 2 to 4 dB/m depending on the relative humidity.¹⁵ Absorption should not affect the SPL comparisons at given frequency, but it is expected to have a small effect on the OASPL comparisons by producing a larger attenuation of OASPL in cases with larger high-frequency content. We have not corrected our data for absorption because the effect is relatively small and depends on humidity, which we did not measure.

For each measurement location, the power spectrum was computed according to

$$S(f) = S_{\text{raw}}(f) + \Delta S_{\text{fr}}(f) + \Delta S_{\text{ff}}(f, \phi) \quad (4)$$

where $S_{\text{raw}}(f)$ is the raw spectrum, $\Delta S_{\text{fr}}(f)$ is the frequency-response correction, and $\Delta S_{\text{ff}}(f, \phi)$ is the free-field correction. The SPL spectrum was then computed according to Eq. (3) and the OASPL according to Eq. (2), with the limits of integration from 0.5 to 150 kHz. The difference in OASPL computed using Eq. (1) (with the uncorrected p'_{rms}) from that given by Eq. (2) is at most 2 dB. In the sections that follow, frequency is presented in its nondimensional form of Strouhal number $St = f D_1 / U_1$.

Equal-Thrust Scaling

Application of the Mach wave elimination technique is accompanied by an increase in thrust and attendant generation of new sources of sound. Because of the complex interaction of the coflow with the primary jet, the effect of the coflow on the noise field is not additive. To assess the impact of Mach wave elimination on the sound field, it is important to compare flows at equal thrust while preserving the essential physics of the problem. To this end, we used simple geometric scaling and maintained constant the velocity, density, and Mach number. With these parameters fixed, the sound intensity p^2 at a fixed radial and polar position scales directly with D^2 (Ref. 16). The nozzle thrust at fixed Mach number and pressure also scales with D^2 . For constant thrust, we compared the untreated jet with the treated jet scaled down (in diameter) by the square root of the thrust ratio F_{1+2}/F_1 . The sound intensity of the treated jet is, thus, divided by F_{1+2}/F_1 , and the resulting correction in terms of SPL is

$$\Delta \text{SPL} = -10 \log_{10}(F_{1+2}/F_1)$$

For a thrust ratio of 1.92 (case B), the correction is -2.8 dB. The same correction applies to the OASPL data. It is important to note that no assumptions, such as a power-law dependence of sound intensity on velocity, are involved in deriving the thrust correction described and, therefore, the equal-thrust data are based solely on the noise data that we measured.

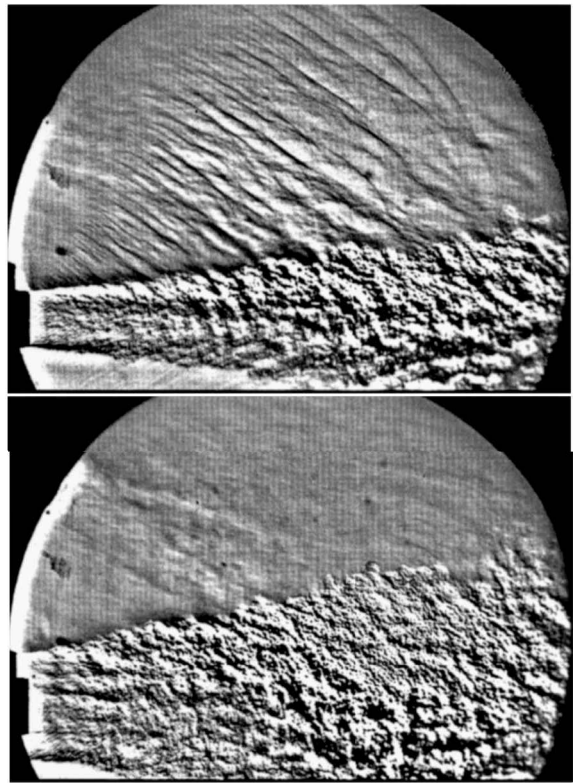


Fig. 4 Schlieren visualizations of cases A (top) and B (bottom).

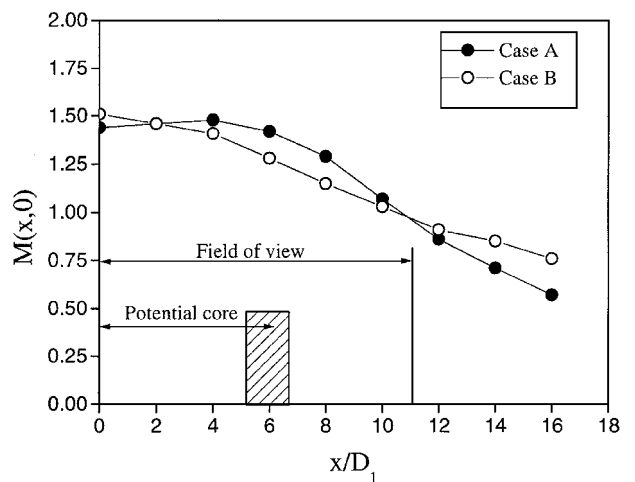


Fig. 5 Centerline Mach number distributions for cases A and B.

IV. Global Features of the Jet

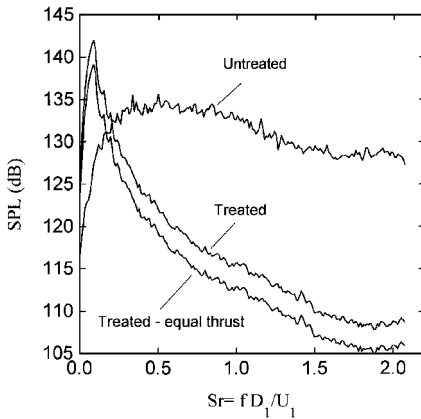
Figure 4 shows schlieren images of the jets of cases A and B. For the untreated jet (case A), the Mach waves are inclined at a slope of approximately 30 deg, from which we infer that eddies travel with Mach number 2.0, and velocity of 700 m/s, with respect to the ambient air. The propagation vector of the Mach waves is, thus, inclined at 60 deg with respect to the jet axis. Application of the coflow (case B) eliminates the Mach waves from the visible field. Both cases A and B have a substantial growth rate, which is an effect of the low density (high effective temperature) of the primary stream, similar to that observed in subsonic shear layers with helium flowing into air.¹⁷ Cold jets, on the other hand, spread very slowly; thus, they do not represent accurately the exhaust of an engine. Figure 5 shows the centerline Mach number distributions for cases A and B, calculated from the pitot measurements. The coflow has relatively minor impact on the axial decay of Mach number. The potential core ends within $x/D_1 = 6$, which is approximately one-half of the field of view of the images presented here. It is notable

that significant Mach waves are generated past the potential core, as seen in Fig. 4.

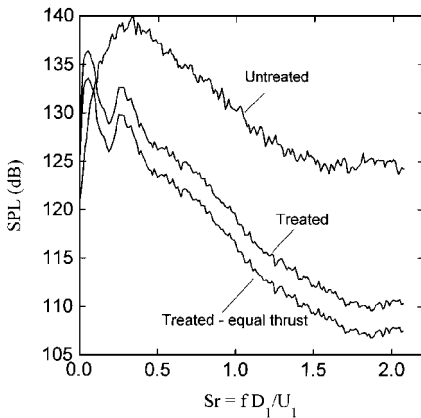
V. Noise Characteristics

Cases A and B

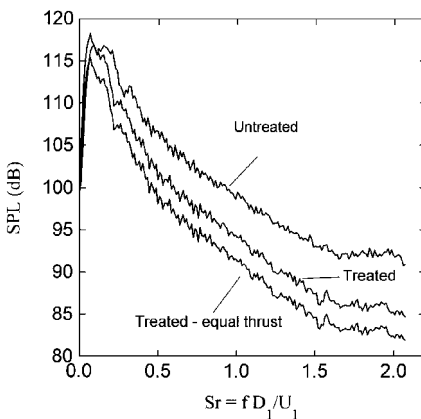
We begin our discussion with the SPL spectra at the peak directivity angle and at various radial locations. Figure 6a shows the very near-field spectrum at $r/D_1 = 3$. The untreated jet has a flat spectrum, indicating equal contribution of large and small scales toward noise generation. Application of treatment suppresses dramatically the middle- and high-frequency components of the spectrum, whereas there is an increase of the very low-frequency components. That increase is due to the proximity (within a few millimeters) of the microphone to the edge of the coflow. The SPL reduction at $Sr = 1.0$ is 18 dB (21 dB at equal thrust). As we move the microphone away to $r/D_1 = 6$ (Fig. 6b), we observe that treatment produces a small increase at the very low frequencies and a reduction of about 14 dB



a) $r/D_1 = 3$ and $\theta = 40$ deg



b) $r/D_1 = 6$ and $\theta = 30$ deg



c) $r/D_1 = 120$ and $\theta = 50$ deg

Fig. 6 SPL spectra of cases A and B at the peak directivity angle.

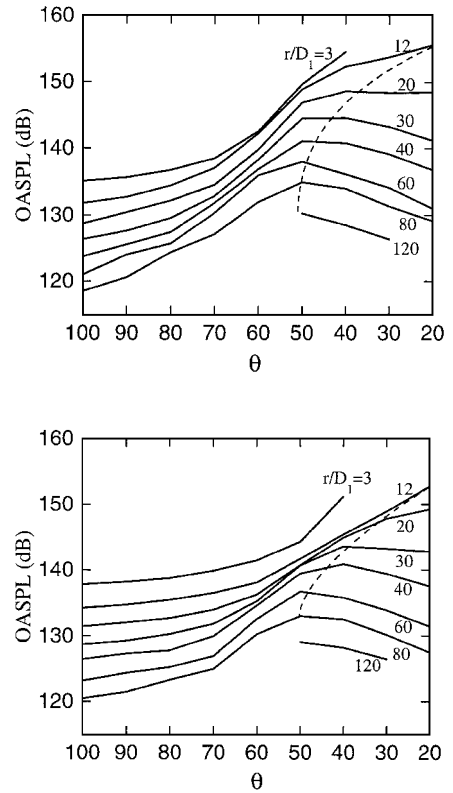


Fig. 7 Spatial distribution of OASPL for cases A (top) and B (bottom); dashed lines indicate approximate trend of peak OASPL.

(17 dB at equal thrust) at the higher frequencies. The OASPL reduction is 8 dB (11 dB at equal thrust). Figure 6c shows the far-field spectra at $r/D_1 = 120$. Treatment reduces the high-frequency components by about 6 dB (9 dB at equal thrust), whereas the very low-frequency components undergo a slight reduction. The reduction in OASPL is 2 dB (5 dB at equal thrust). The spectrum peaks at a very low Strouhal number of about 0.15 ($f = 10$ kHz), which suggests Mach wave radiation from very large eddies well past the potential core and/or emission of subsonic sources far downstream of the jet exit. It is important to realize that the low-frequency part of the spectrum, $0 < Sr < 0.25$, is not very significant to full-scale engine noise, a point further discussed at the end of this section. The small reduction of sound at very low frequencies suggests that far-field Mach waves were not completely suppressed or that low-frequency noise originates primarily from subsonic sources.

Next we examine the variation of OASPL with radial and polar positions for cases A and B, shown in Fig. 7. The untreated and treated flows share the same trends: at small distances OASPL peaks at low angles, whereas at large distances it peaks at $\theta = 50$ deg. Whereas this is close to the visually observed Mach wave propagation at 60 deg, it would also be consistent with the directivity of a low-speed jet.¹⁶ In other words, far-field directivity of the OASPL may be influenced by subsonic sources of noise. To examine the directivity of supersonic sources of noise, which we suspect occupy the high-frequency part of the spectrum, we plot the spatial distribution of sound in the range $1.2 < Sr < 1.6$ in Fig. 8. For the untreated case, the far-field directivity peaks at 60 deg, consistent with the direction of the Mach waves. For the treated case, that peak is greatly suppressed, consistent with elimination of Mach waves. These findings, combined with the noise reduction seen in the spectra of Fig. 6c, indicate that Mach waves constitute a significant component of the far-field noise at Strouhal numbers larger than about 0.5.

The Strouhal number corresponding to the peak value of the SPL spectrum, Sr_{peak} , is plotted vs r and θ in Fig. 9. For the untreated jet, the general trend is a decrease in Sr_{peak} with increasing r and decreasing θ , with exception of the near field ($r/D_1 = 3$), where Sr_{peak} becomes large at small θ , consistent with high-frequency, intense Mach wave emission close to the jet. Elimination of Mach waves changes this near-field trend dramatically, rendering it similar

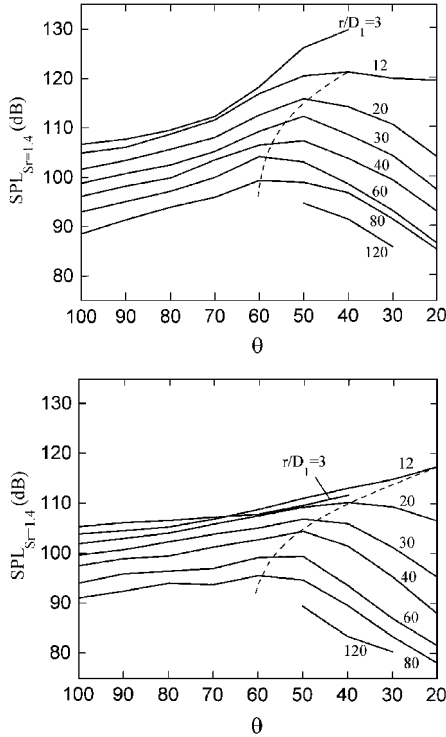


Fig. 8 Spatial distribution of high-frequency component of spectrum for case A (top) and case B (bottom); dashed lines indicate approximate trend of peak SPL.

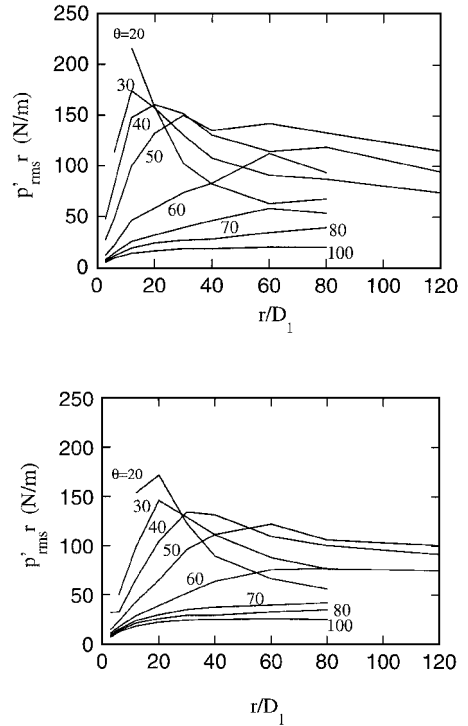


Fig. 10 Spatial variation of the product $p'_{rms} r$ for cases A (top) and B (bottom); spectra at $r/D_1 = 120$ and $\theta = 50$ deg for cases A and C.

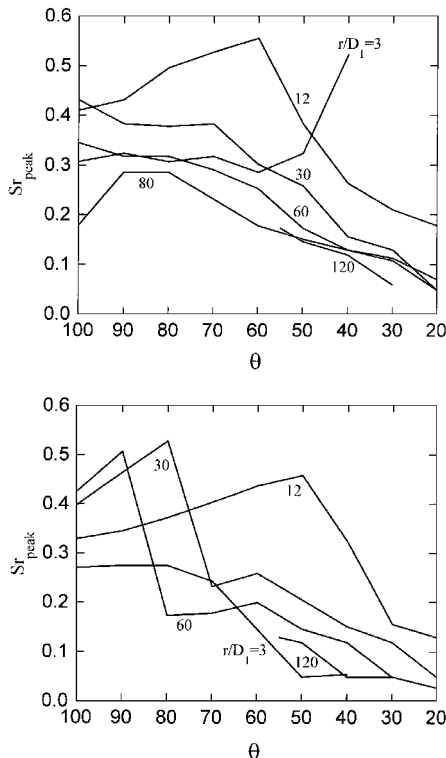


Fig. 9 Spatial distribution of Strouhal number at spectrum peak for cases A (top) and B (bottom).

to the far-field trend noted earlier. There is an appreciable overall decrease in Sr_{peak} when treatment is applied.

Identification of the far field is a concern for any jet noise experiment. The far field is supposed to be far away from all of the sources of noise.¹⁶ In the far field, the pressure fluctuation along a given azimuthal direction should decay with distance according to $p'_{rms} \sim 1/r$, or $p'_{rms} r = const$. To test this relation, we plot $p'_{rms} r$ vs r and θ in Fig. 10. For both the treated and untreated cases,

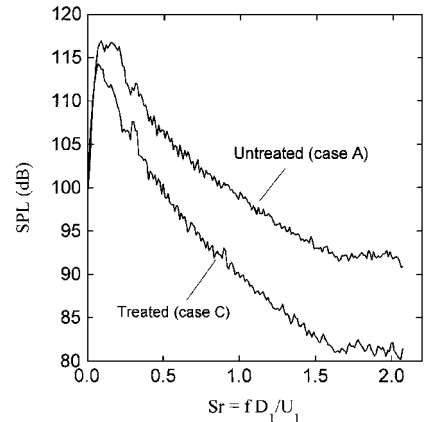


Fig. 11 Spectra at $r/D_1 = 120$ and $\theta = 50$ deg for cases A and C.

it reaches near-constant values for $r/D_1 > 60$. The small decay of case A for $r/D_1 > 80$ may be due to sound absorption, which is expected to impact case A more than case B (see related discussion in Sec. III). We are, thus, confident that the surveys done at $r/D_1 = 80$ and 120 are indeed in the far field. Note that there is significant addition of noise sources, indicated by an increase in $p'_{rms} r$, up to $r/D_1 = 40$.

Cases C and D

Addition of the coflow to the primary jet alters the fluid dynamics of the situation, particularly when the coflow has substantial momentum flux, as in case B. This in turn changes the distribution and strength of the quadrupole sources of noise, an effect that may interfere with the effect of Mach wave elimination. In an additional effort to isolate the impact of Mach wave elimination, we tested case C, which has a coflow at very low velocity and high speed of sound, supplied by a large nozzle with $D_2/D_1 = 4.0$. Here the coflow has very low momentum flux, and so it should not alter the fluid dynamics of the jet, besides eliminating its Mach waves. The far-field spectrum of case C is compared with that of the untreated jet (case A) in Fig. 11. Equal-thrust correction is very small here (0.5 dB), and so it is omitted. There is noise reduction across the

Downloaded by Dimitri Papamoschou on January 30, 2014 | http://arc.aiaa.org | DOI: 10.2514/6.2014-702

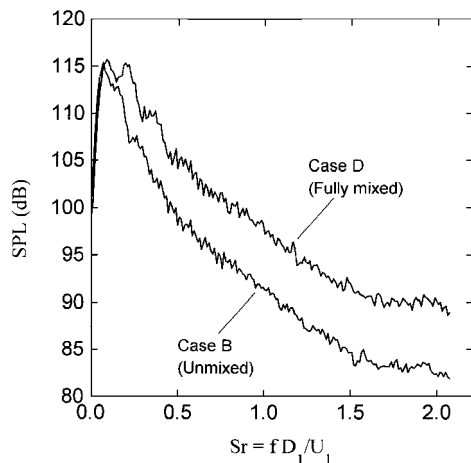


Fig. 12 Spectra at $r/D_1 = 120$ and $\theta = 50$ deg for unmixed coaxial jet (case B) and fully mixed single jet (case D).

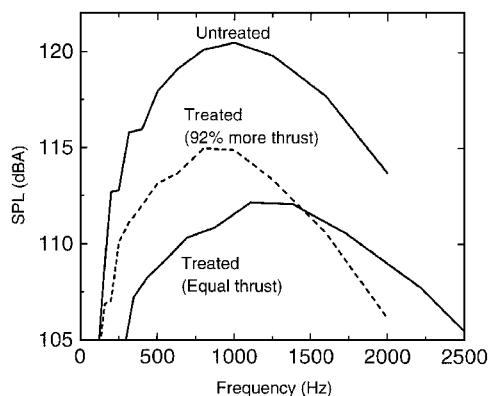


Fig. 13 A-weighted, 1/3-octave spectra for cases A and B, scaled to a full-size engine.

entire spectrum. The high-frequency part of the spectrum is reduced by about 9 dB, which is roughly the same reduction achieved in case B with equal-thrust scaling (Fig. 6c). This indicates that most if not all of the high-frequency noise reduction in case B resulted from elimination of Mach waves. Case C provides strong evidence that Mach waves constitute the dominant source of noise at the higher end of the spectrum, which, as we will subsequently examine, is most relevant to aircraft noise. In terms of sound intensity, the contribution of Mach waves is at least 85% of the total sound field at those frequencies.

In several engine designs, the coflow (fan) and primary (core) streams are mixed before exhausting from the nozzle. We felt that it was important from a propulsive viewpoint (not so much a physical viewpoint) to examine the noise characteristics of a fully mixed jet. A thermodynamic calculation shows that mixing the primary and coflow streams in the proportions of case B, and accelerating the mixture to Mach 1.5, yields an exit velocity $U_1 = 700$ m/s and effective temperature $T_1/T_\infty = 1.8$. We simulated this jet, case D, by increasing the mass fraction of air in the helium-air mixture and expanding perfectly the mixture through our Mach 1.5 nozzle. Because of its lower velocity, case D has weaker Mach wave emission than case A; hence, the physics of the problem are now different. In the equal-thrust comparison of cases D and B, shown in Fig. 12, it is seen that the unmixed case B has a substantial benefit, about 7 dB at the high frequencies, over the fully mixed case D. This suggests that an unmixed core-fan exhaust at Mach wave elimination conditions will be beneficial compared to a mixed exhaust. One should also keep in mind that high-speed mixing causes significant thrust losses, not just from the drag of the mechanical mixers but also from the total pressure loss due to mixing itself.¹⁸

Impact on Aircraft Noise

The relevance of noise measurements cannot be fully assessed without incorporating the element of human perception of sound. For aircraft noise, this is commonly done using the perceived noise level (PNL) metric.¹⁹ The small scale of our experiments (about 1/80 scale) prevents us from computing the PNL because our frequencies, scaled to a full-size engine, range only up to 2500 Hz, whereas the PNL calculation requires the full audible range up to 20 kHz. Instead, we use the simpler metric of A-weighted decibels (dBA),¹⁹ which features a frequency weighting similar to that used in the PNL metric. First, we divided our frequencies by the scaling factor of 80 to scale up our results to a jet diameter $D_1 = 1$ m. Then, we computed the 1/3-octave spectrum and added the dBA correction to it. The resulting far-field spectra for cases A and B are shown in Fig. 13. They peak at about 1000 Hz, which corresponds to $Sr = 1.0$, i.e., the portion of the spectrum heavily influenced by Mach waves. For equal thrust, the treated flow provides a noise reduction of about 9 dBA at 1000 Hz. This indicates that Mach waves affect strongly the sensitive part of the audible spectrum.

VI. Conclusions

Noise surveys of Mach 1.5 jets with coflow at Mach wave elimination conditions have been performed. Elimination of Mach waves from a jet with velocity of 920 m/s leads to a dramatic reduction of the near-field noise (11-dB OASPL, 20 dB at middle and high frequencies) and an appreciable reduction of the far-field noise (5-dB OASPL, 9 dB at frequencies most relevant to aircraft noise). Our measurements suggest that, in a full-scale engine, Mach waves would constitute at least 85% (9 dB) of the sound field to which the human ear is most sensitive. The far-field directivity of the OASPL is in fair, but not very good, agreement with the propagation direction of Mach waves as visualized in schlieren pictures. In contrast, the far-field directivity of the high-frequency part of the spectrum is in excellent agreement with the visualized propagation of the Mach waves. At the same exit Mach number, the unmixed combination of jet and coflow is quieter than the fully mixed combination.

Acknowledgments

The support by NASA Lewis Research Center is gratefully acknowledged (Grant NAG-3-1981 monitored by Milo Dahl). We thank Erina Murakami for her assistance with the data acquisition and control part of the experiment.

References

- McLaughlin, D. K., Morrison, G. D., and Troutt, T. R., "Experiments on the Instability Waves in a Supersonic Jet and Their Acoustic Radiation," *Journal of Fluid Mechanics*, Vol. 69, No. 11, 1975, pp. 73-95.
- Troutt, T. R., and McLaughlin, D. K., "Experiments on the Flow and Acoustic Properties of a Moderate Reynolds Number Supersonic Jet," *Journal of Fluid Mechanics*, Vol. 116, March 1982, pp. 123-156.
- Tam, C. K. W., and Burton, D. E., "Sound Generated by Instability Waves of Supersonic Flows. Part 2. Axisymmetric Jets," *Journal of Fluid Mechanics*, Vol. 138, Jan. 1984, pp. 249-271.
- Seiner, J. M., Bhat, T. R. S., and Ponton, M. K., "Mach Wave Emission from a High-Temperature Supersonic Jet," *AIAA Journal*, Vol. 32, No. 12, 1994, pp. 2345-2350.
- Mitchell, B. E., Lele, S. K., and Moin, P., "Direct Computation of Mach Wave Radiation in an Axisymmetric Supersonic Jet," *AIAA Journal*, Vol. 35, No. 10, 1994, pp. 1574-1580.
- Bishop, K. A., Ffowcs Williams, J. E., and Smith, W., "On the Noise Sources of the Unsuppressed High-Speed Jet," *Journal of Fluid Mechanics*, Vol. 50, Pt. 1, 1971, pp. 21-32.
- Powell, A., "On the Noise Emanating from a Two-Dimensional Jet Above the Critical Pressure," *Aeronautical Quarterly*, Vol. 4, Feb. 1953, pp. 103-122.
- Tam, C. K. W., "On the Noise of Nearly Ideally Expanded Supersonic Jet," *Journal of Fluid Mechanics*, Vol. 51, Pt. 1, 1972, pp. 69-96.
- Papamoschou, D., "Mach Wave Elimination from Supersonic Jets," *AIAA Journal*, Vol. 35, No. 10, 1997, pp. 1604-1611.
- Papamoschou, D., and Bunyajitradulya, A., "Evolution of Large Eddies in Compressible Shear Layers," *Physics of Fluids*, Vol. 4, No. 3, 1997, pp. 756-765.
- Tanna, H. K., "Coannular Jets—Are They Really Quiet and Why?" *Journal of Sound and Vibration*, Vol. 72, No. 1, 1980, pp. 97-118.

¹²Dosanjh, D. S., Yu, J. C., and Abdelhamid, A. N., "Reduction of Noise from Supersonic Jet Flows," *AIAA Journal*, Vol. 9, No. 12, 1971, pp. 2346–2353.

¹³Dahl, M. D., and Morris, P. J., "Noise from Supersonic Coaxial Jets, Part 2: Normal Velocity Profile," *Journal of Sound and Vibration*, Vol. 200, No. 5, 1997, pp. 665–699.

¹⁴Kinzie, K. W., and McLaughlin, D. K., "An Experimental Study of Noise Radiated from Supersonic Elliptic Jets," AIAA Paper 95-0511, Jan. 1995.

¹⁵Bass, H. E., Sutherland, L. C., Blackstock, D. T., and Hester, D. M., "Atmospheric Absorption of Sound: Further Developments," *Journal of the Acoustical Society of America*, Vol. 97, No. 1, 1995, pp. 680–683.

¹⁶Goldstein, M. E., *Aeroacoustics*, 1st ed., McGraw-Hill, New York, 1976, pp. 38 and 93.

¹⁷Davey, R. F., and Roshko, A., "The Effect of a Density Difference on Shear-Layer Instability," *Journal of Fluid Mechanics*, Vol. 53, No. 3, 1972, pp. 523–543.

¹⁸Papamoschou, D., "Entropy Production and Pressure Variation in Confined Turbulent Mixing," *AIAA Journal*, Vol. 31, No. 9, 1993, pp. 1643–1650.

¹⁹Smith, M. J. T., *Aircraft Noise*, 1st ed., Cambridge Univ. Press, Cambridge, England, UK, 1989, pp. 4–19.

M. Samimy
Associate Editor